JOURNAL OF Materials CHEMISTRY

Li mobility in triclinic and rhombohedral phases of the Nasicon-type compound $LiZr_2(PO_4)_3$ as deduced from NMR spectroscopy

K. Arbi,[a] M. Ayadi-Trabelsi[b] and J. Sanz*[a]

[a]*Instituto de Ciencia de Materiales de Madrid (ICMM), Consejo Superior de Investigaciónes Científicas (CSIC), Cantoblanco, 28049 Madrid, Spain. E-mail: jsanz@icmm.csic.es*
[b]*Laboratoire PCM, Faculté de Sciences de Bizerte, Zarzouna 7021, Tunisia*

Received 10th April 2002, Accepted 21st June 2002
First published as an Advance Article on the web 9th August 2002

The Nasicon-type $LiZr_2(PO_4)_3$ compound exhibits, around 310 K, a first order transition from the triclinic $C\bar{1}$ to the rhombohedral $R\bar{3}c$ form, which has been followed by DSC, XRD and NMR (^{31}P and ^{7}Li) techniques. During heating–cooling treatments a hysteresis cycle was detected in which triclinic and rhombohedral phases coexist. In the low-temperature triclinic form, the four-fold coordination of Li deduced from neutron diffraction experiments, at midway positions between M_1 and M_2 sites, was confirmed. From relaxation NMR data, a microscopic activation energy of $E_m = 0.43$ eV was measured in the triclinic phase. Above the phase transition a strong delocalisation of Li over structural sites disposed along conduction paths was detected. The high mobility of Li detected in the high-temperature form explains the outstanding conductivity reported for the rhombohedral phase.

Introduction

Lithium-ion conducting solids are materials of increasing interest because of their possible use as solid electrolytes in high-energy solid-state batteries. Nasicon[1] materials of formula $LiM_2(PO_4)_3$, where M = Ge, Ti, Sn, Hf, Zr, have been extensively studied[2–6] because of their good ionic conductivity. The framework of these compounds is built up by $M_2(PO_4)_3$ units in which two MO_6 octahedra and three tetrahedral PO_4 share oxygen atoms. The $[MO_6][(PO_4)_3][MO_6]$ units alternate with the alkali cations to make infinite chains parallel to the ternary axis of the structure (*c*-axis). Each PO_4 tetrahedron shares its oxygens with four MO_6 of three $M_2(PO_4)_3$ units to form the Nasicon's framework. In this structure, alkali cations can diffuse along a three-dimensional network of conduction paths, where they can be accommodated at different sites.

In $LiGe_2(PO_4)_3$ and $LiTi_2(PO_4)_3$ compounds, a rhombohedral symmetry (space group $R\bar{3}c$) was deduced from X-ray (XRD) and neutron diffraction (ND) experiments.[7,8] In this phase Li ions are octahedrally coordinated at the intersection of three conduction channels (M_1 sites). When the ionic radii of the tetravalent cation M^{4+} become bigger (M = Sn, Hf, Zr), a triclinic distortion was detected[9–11] that disappeared when samples were heated above the phase transition temperature.

Concerning $LiZr_2(PO_4)_3$, Sudreau *et al.*[5] concluded from NMR and XRD analysis that the symmetry of the low-temperature form was monoclinic (space group *Cc*). Later, a detailed indexing of the powder X-ray diffraction pattern of $LiZr_2(PO_4)_3$ confirmed the triclinic symmetry for this phase.[12] Finally, neutron diffraction studies of low- and high-temperature forms[11,13] of $LiZr_2(PO_4)_3$ confirmed triclinic and rhombohedral symmetries for the two related phases. In the triclinic phase (called α'), this study showed that the Li ions occupy, with probabilities 0.71 and 0.29, Li(1) and Li(2) positions between M_1 and M_2 sites (see Fig. 1). In the rhombohedral phase (called α), Li^+ ions are distributed over six equivalent positions around M_1 sites making detection difficult with diffractometric techniques. Structural analysis carried out in both phases confirmed different mobilities proposed for Li in the two forms.

In this work, structural sites and the mobility of Li^+ ions in $LiZr_2(PO_4)_3$ are analyzed by ^{7}Li NMR spectroscopy. For that, the triclinic–rhombohedral transition has been previously characterized with DSC, XRD and ^{31}P MAS-NMR techniques. Obtained results permit a better understanding of the conductivity data reported on this compound.[5]

Experimental section

The sample of $LiZr_2(PO_4)_3$ was prepared by the ceramic method. Stoichiometric amounts of Li_2CO_3, ZrO_2 and

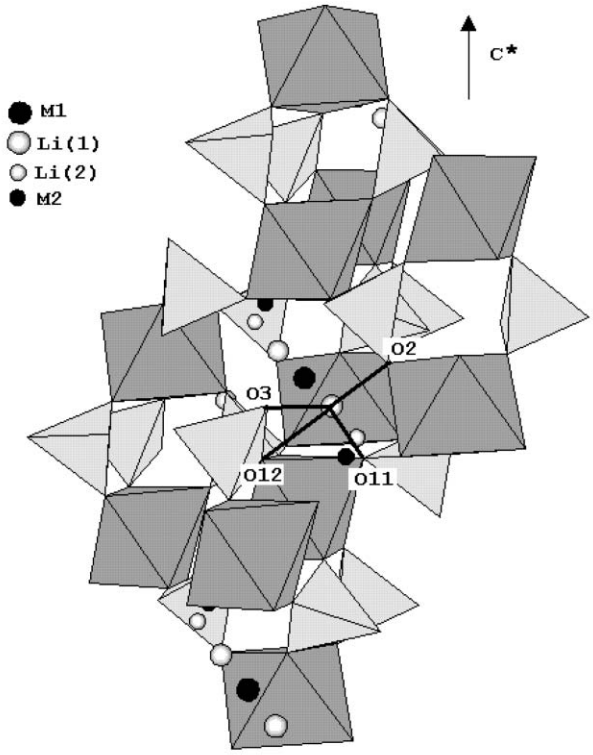

Fig. 1 Structure of the triclinic phase of $LiZr_2(PO_4)_3$ in which conduction paths are visualized. Li(1) and Li(2) sites, deduced from ND studies, have also been included.

$(NH_4)_2HPO_4$ were first dried at 120 °C for 10 h and then mixed and treated in a platinum crucible at 180, 300, 500, 700, 900 and 950 °C. After each treatment, the mixture was ground using an agate mortar and analyzed by X-ray diffraction. The samples were stored for later use when the characteristic peaks of reagents and/or intermediate compounds such as pyrophosphates were not detected.

A differential scanning calorimeter (Seiko 220 CU) was used to analyze the phase transformation of $LiZr_2(PO_4)_3$. The experiment was carried out under a static air atmosphere between −60 and 100 °C with heating and cooling rates of 10 °C min^{-1}. The estimated error on enthalpy values was lower than 0.1 J g^{-1}.

X-Ray powder diffraction patterns were recorded at different temperatures in the range of 20–70 °C using a high-temperature AP HTK10 camera adapted to a PW 1050/25 Phillips diffractometer. In cooling and heating experiments, the sample was kept at each temperature for 5 min before recording XRD patterns with Cu-Kα radiation (λ = 1.5405981 Å). Data were collected in the 2θ range 12–40° with a step size of 0.02° and a counting time of 0.1 s $step^{-1}$.

^{31}P and ^{7}Li NMR spectra recorded under static and MAS conditions were obtained at different temperatures between 18 and 80 °C using a B-VT 1000/SU07 unit adapted to an MSL 400 Bruker spectrometer. The frequencies used for ^{31}P and ^{7}Li were 161.97 and 155.50 MHz, respectively. Spectra were taken after a π/2 pulse irradiation and the interval between successive scans chosen to avoid saturation effects (20–30 s). In the MAS-NMR experiments, the spinning rate of samples was 4 kHz. In all cases, the number of accumulations was 10. ^{7}Li and ^{31}P chemical shift values were given relative to 1 M LiCl and 85% H_3PO_4 aqueous solutions. The fitting of NMR spectra was carried out using the Bruker WINFIT software package.[14] This program allows the position, line width and intensity of components to be determined with a non-linear, least-squares iterative method; however, quadrupole C_Q and η values have to be deduced with a trial and error procedure. For quantitative purposes, the sum of the integrated intensities of spinning sidebands of each component was calculated. ^{7}Li spin-lattice (T_1) relaxation times of $LiZr_2(PO_4)_3$ were obtained between −70 and 100 °C with the π–τ–π/2 sequence. Reciprocal spin-spin relaxation times values (T_2^{-1}) were deduced from the full-width at half-height (FWHH) of the NMR lines. In the case of Gaussian lines, T_2^{-1} values were calculated as 0.6π × FWHH; in the case of Lorenzian lines, T_2^{-1} were calculated as π × FWHH.

Results and discussion

Phase transition

Calorimetric curves obtained during the heating and cooling runs of $LiZr_2(PO_4)_3$ are shown in Fig. 2. During heating experiments, an endothermic peak was detected at *ca.* 51 °C with an enthalpy of 13.2 J g^{-1}. In cooling treatments, an exothermic peak was detected at 33 °C. The enthalpy corresponding to this peak was −11.5 J g^{-1}. The position of the high temperature peak shifted towards slightly lower temperatures, decreasing the separation between two peaks, in subsequent heating and cooling cycles (not shown in Fig. 2)

X-Ray diffraction patterns of $LiZr_2(PO_4)_3$, recorded between 20 and 70 °C, are shown in Fig. 3. In agreement with previous results,[12] the phase detected at room temperature displays a triclinic distortion (space group $C\bar{1}$), with unit cell parameters a = 15.079 Å, b = 8.855 Å, c = 9.123 Å, α = 89.7°, β = 123.95° and γ = 90.44°. In the case of the rombohedral phase (space group $R\bar{3}c$), obtained above 50 °C, unit cell parameters are a = 8.85493 Å and c = 22.1440 Å.[13]

In the temperature range 35–55 °C, the triclinic and rhombohedral phases coexist in the XRD patterns.[15] The

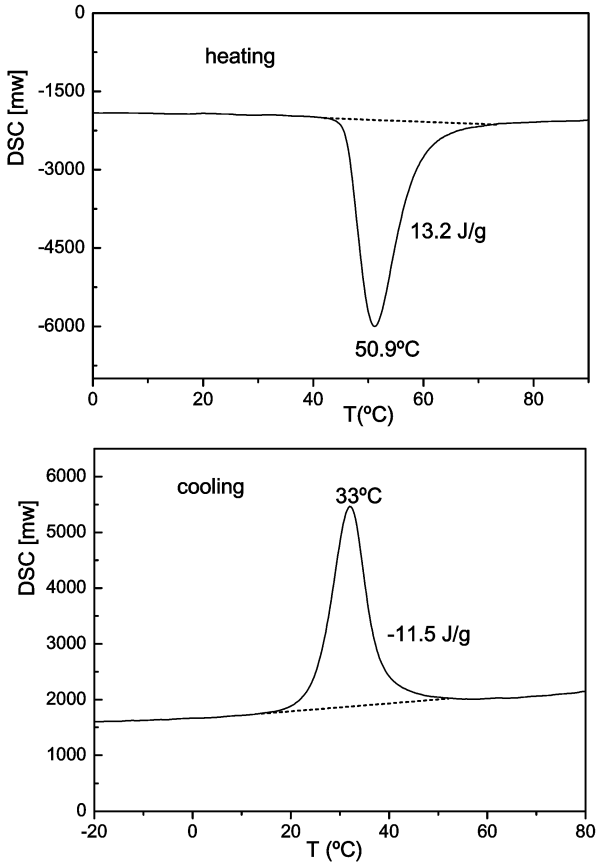

Fig. 2 DSC curves of $LiZr_2(PO_4)_3$, recorded during heating and cooling treatments.

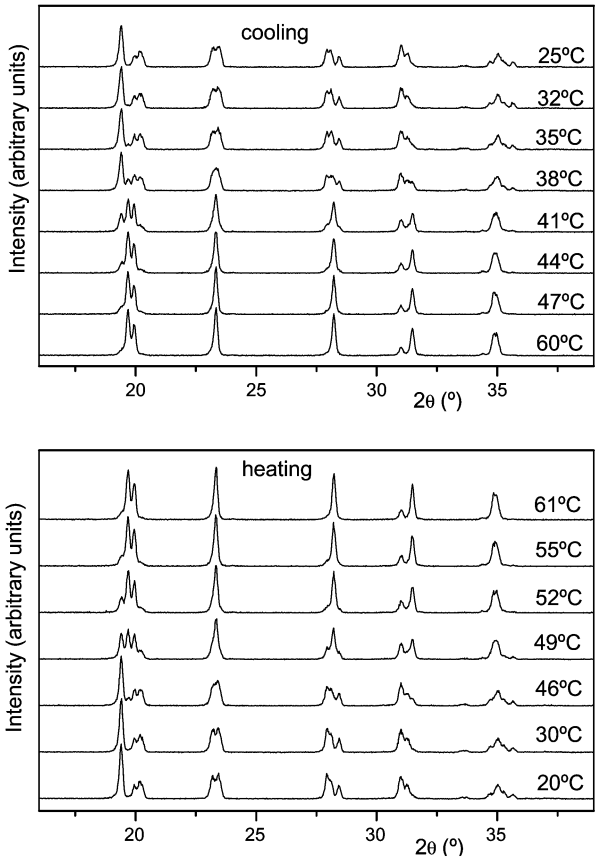

Fig. 3 X-Ray diffraction patterns of $LiZr_2(PO_4)_3$ taken at the indicated temperatures during heating–cooling treatments.

most important changes detected during heating–cooling treatments are produced in the 2θ range 19–21°; below 35 °C three peaks were detected at 19.4, 19.9 and 20.2°, however, above 40 °C a new peak at $2\theta \approx 19.7°$ was observed. Peaks at 19.4 and 20.2° disappear gradually with heating, the XRD patterns of the sample heated at 60 °C displaying only the two inner peaks at 19.7 and 19.96°. During this transformation, other changes were also observed: relative intensities of the two components at $2\theta \approx 31°$ are exchanged, and doublets observed at $2\theta \approx 23$ and 28° become a single peak above 45 °C. During cooling treatments, the opposite modifications were detected but shifted towards lower temperatures. The coexistence of the two phases in an appreciable temperature interval suggests that the observed first-order transition displays a martensitic character. The presence of domains that have different transition temperatures explains the existence of two phases during the transition. According to results showed here, formation of rhombohedral domains from small triclinic ones is more difficult than the splitting produced during cooling treatments, explaining the hysterisis loop observed during heating–cooling treatments. Similar results were reported previously for the $LiSn_2(PO_4)_3$ phosphate.[3,9]

^{31}P NMR spectra recorded at different temperatures are shown in Fig. 4. At room temperature, the spectra are formed by the three lines at −22.2, −23.6 and −24.1 ppm ascribed to three crystallographic sites of the triclinic phase.[11] Up to and above 40 °C, the intensity of the −22.2 and −23.6 ppm lines decreases progressively. When the structural transition was achieved, the ^{31}P MAS-NMR spectrum is formed by a single component at −24 ppm ascribed to the unique site occupied by phosphorus in the rhombohedral structure.[13] Small peaks near −22 ppm have been assigned to the presence of an amorphous secondary phase. During cooling treatments, the opposite behavior was detected. From the intensity of ^{31}P NMR lines, the relative proportion of the rhombohedral phase as a function of the temperature was deduced (Fig. 4, bottom). During heating treatments, the rhombohedral phase was preponderant above 50 °C; however, during cooling treatments the triclinic

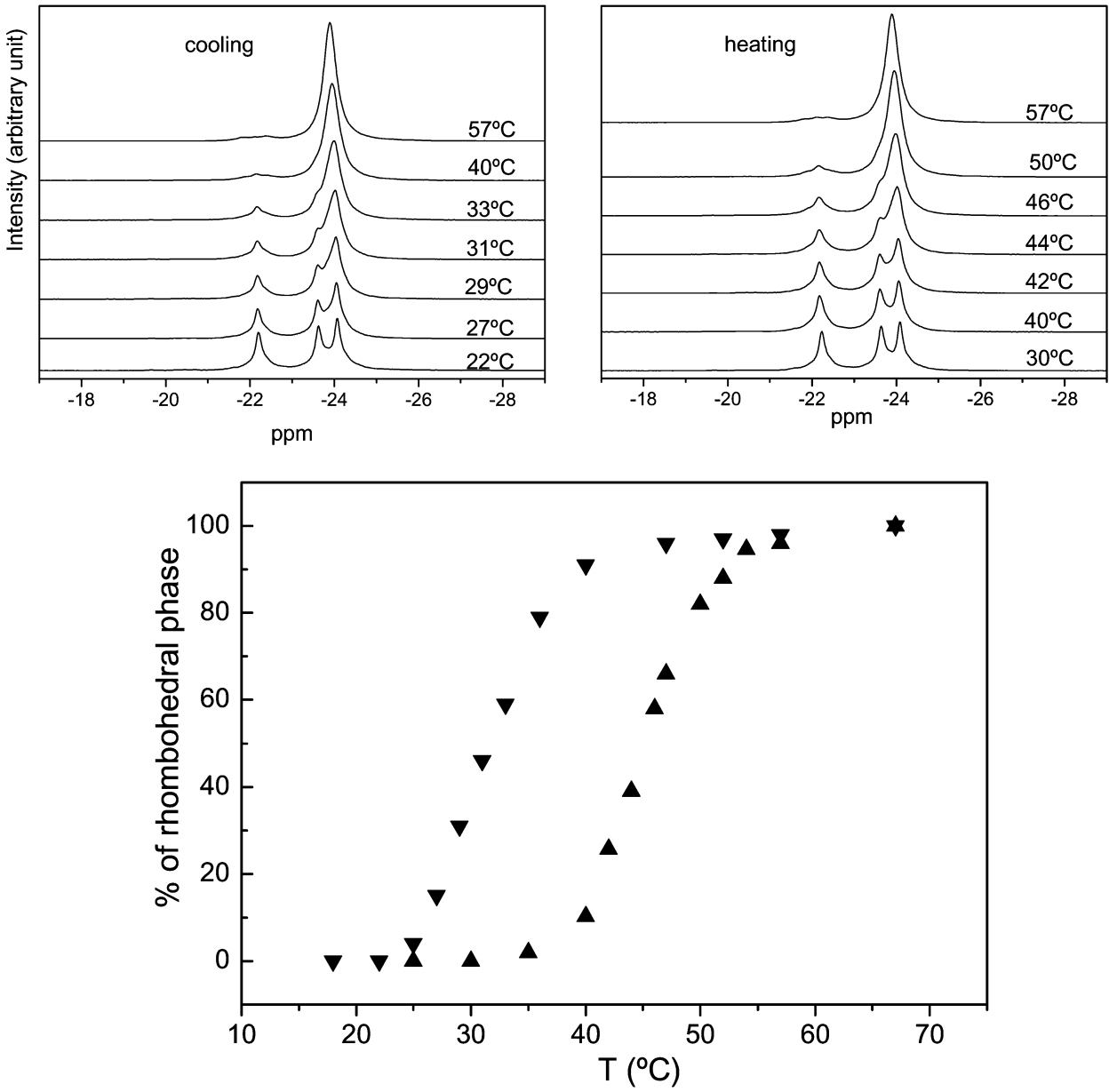

Fig. 4 ^{31}P MAS-NMR spectra of $LiZr_2(PO_4)_3$ recorded at different temperatures (top). Relative proportion of the rhombohedral phase *vs.* temperature, as deduced from ^{31}P MAS-NMR spectra (bottom). Up and down triangles correspond to data taken during heating and cooling treatments, repectively.

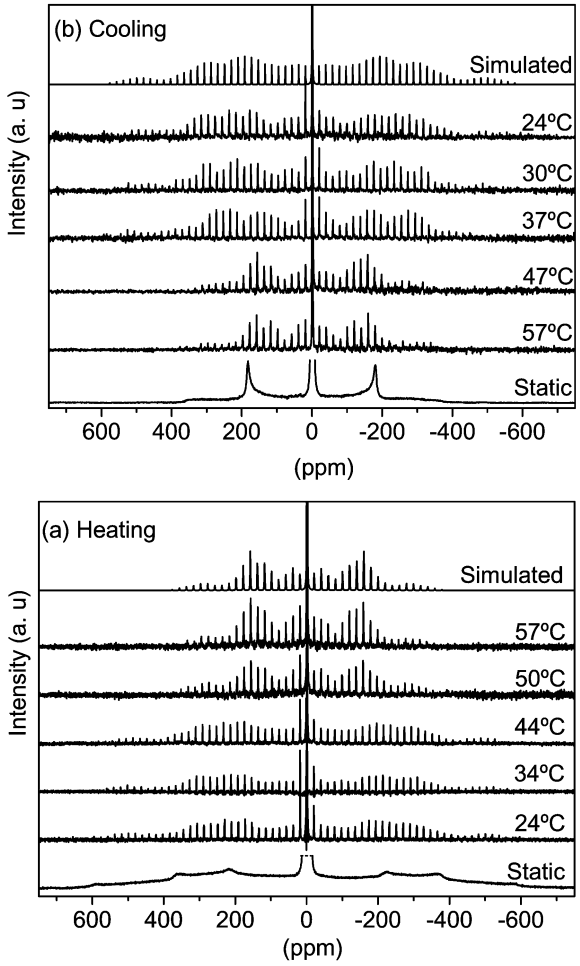

Fig. 5 ^{7}Li MAS-NMR spectra of $LiZr_2(PO_4)_3$ recorded at indicated temperatures during heating (a) and cooling (b) treatments. Static spectra of low- and high-temperature forms are included at the bottom of (a) and (b). For the sake of clarity, central peaks of the static spectra were cut off. Calculated MAS-NMR spectra of rhombohedral and triclinic forms are given at the top of the same figures.

phase was only the major phase below 27 °C. These observations confirm the hysteresis loop detected with DSC and XRD techniques.

Li mobility

^{7}Li (I = 3/2) NMR spectra of $LiZr_2(PO_4)_3$, recorded at different temperatures, are given in Fig. 5. ^{7}Li static NMR spectra, obtained at room temperature, are formed by a central (−1/2, 1/2) line and two satellite transitions (±1/2, ±3/2) that produce small shoulders at both sides of the maximum [spectra at the bottom of Fig. 5(a) and 5(b)]. In the case of the ^{7}Li MAS-NMR spectra, central and satellite transitions are modulated by narrow spinning sidebands, and this favors the detection of the quadrupole pattern (see Fig. 5). ^{7}Li NMR spectra of $LiZr_2(PO_4)_3$ recorded at $T > 50$ °C are clearly different from those recorded at $T < 40$ °C indicating that Li^+ ions change their position when going from the triclinic to the rhombohedral phase. In the triclinic phase, satellite transitions in static ^{7}Li NMR spectra display three broad shoulders; however, in the rhombohedral phase the same transitions display only two shoulders at both sides of the central transition[16] [see bottom spectra of Fig. 5(a) and 5(b)].

By fitting the static and MAS-NMR spectra, quadrupole C_Q and η constants related to principal values of the electrical field tensor at structural sites occupied by lithium were determined. From these values, point symmetry and polyhedra distortions can be estimated.[16] In the case of the rhombohedral phase, structural sites occupied by lithium display axial symmetry (C_Q = 110 kHz and η = 0), but in the triclinic phase, lithium sites have a lower symmetry (C_Q = 186 kHz and η = 0.3). According to deduced values, distortions produced in Li polyhedra are more important in the triclinic than in the rhombohedral phase.

The ^{7}Li MAS NMR spectrum of the triclinic phase was reproduced with a single site indicating that, contrary to results deduced from ND experiments, Li^+ ions occupy only one type of site. Quadrupole constants deduced in the triclinic form of $LiZr_2(PO_4)_3$ are very similar to those deduced in $LiHf_2(PO_4)_3$, where Li^+ ions occupy Li(1) sites, located between M_1 and M_2 sites[10] (see Fig. 1). Calculated second moment values of the triclinic phase (0.30 G^2) agree reasonably well with those deduced from the central NMR line recorded under static conditions (0.33 G^2), confirming again the occupation of Li(1) sites. These values were deduced from the Van Vleck's expression:[17]

$$\Delta\varpi^2 = \frac{3}{5}\gamma_I^4\hbar^2 I(I+1)\sum_k \frac{1}{r_{jk}^6} + \frac{4}{15}\gamma_i^2\gamma_s^2\hbar^2 S(S+1)\sum_k \frac{1}{r_{jk}^6}$$

where the first term accounts for dipolar interactions between like spins and the second for interactions between unlike spins, γ_I and γ_S are the gyromagnetic ratios for I and S spins and r_{jk} is the distance between interacting spins. In these calculations, it was shown that dipolar Li–P interactions (0.2 G^2) are considerably higher than Li–Li interactions (0.06 G^2).

In the rhombohedral phase, the ^{7}Li NMR signal displays axial symmetry, suggesting that lithium ions occupy M_1 sites located at the ternary axis. However, the static ^{7}Li NMR spectrum of the rhombohedral phase, displays narrowing effects associated with an increase of the Li mobility. According to this fact, the line changes from Gaussian to Lorenzian shape. The increase in Li mobility was supported by the structural analysis of the two related phases: Li–O bond distances increase from 2.09 to 2.27 Å when going from the triclinic to the rhombohedral phase.[11,13] In the last phase, Petit and Sapoval[18] concluded from crystallographic data that the M_1 site splits into six equivalent positions to conserve the D_{3d} symmetry. As a consequence of the lithium delocalization in M_1 cavities, an averaged axial symmetry is detected by ^{7}Li NMR spectroscopy.

In ^{7}Li NMR spectra recorded with the MAS techniques, dipolar interactions are eliminated and the linewidth of central transitions is reduced. From this fact, spectral resolution increases considerably allowing a better analysis of structural sites occupied by lithium in the two crystallographic forms. A comparison of MAS-NMR spectra of the two phases showed that the linewidth of the central transition of the rhombohedral phase is higher than in the triclinic phase (not shown), suggesting that Li ions occupy several sites in the rhombohedral phase and that the central component is the result of averaging effects. According to this fact, the experimental MAS-NMR envelope of the rhombohedral phase could not be fitted with a single component and an additional narrow component, associated with mobile Li species, should be included in the analysis of the spectrum.

The temperature dependence of the spin-lattice relaxation time is given in Fig. 6. In this plot, relaxation T_1^{-1} values remain constant below 250 K, but increase considerably above this temperature. At 310 K, T_1^{-1} values increase sharply as a consequence of the triclinic–rhombohedral transformation. Above the transition, the T_1^{-1} curve attains a broad maximum. In general, the evolution of T_1^{-1} values with temperature can be described with the expression[19,20]

$$T_1^{-1} = C\left[\frac{\tau_c}{1+(\omega\tau_c)^{1+\beta}} + \frac{4\tau_c}{1+(2\omega\tau_c)^{1+\beta}}\right]$$

where C depends on the magnetic interaction that causes the

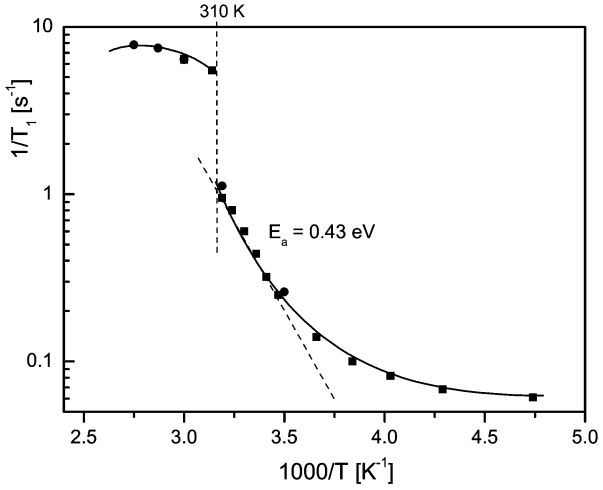

Fig. 6 Temperature dependence of ^{7}Li NMR spin-lattice relaxation rates ($1/T_1$) of $LiZr_2(PO_4)_3$. Circles correspond to heating and squares to cooling treatments. The vertical dashed line corresponds to the triclinic–rhombohedral transition. An activation energy of 0.43 eV was deduced from fitting the experimental points to the dashed line in the triclinic form.

nuclear relaxation and β is a constant that depends on correlation effects in Li motions. When $\beta = 1$, the above expression takes the usual BPP form. Residence times τ_c at structural sites are given by

$$\tau_c = \tau_{c_0} \exp\left(E_M/kT\right)$$

where E_M is the long-range activation energy for the lithium motion. In our case, the fitting of the curve T_1^{-1} is difficult because of the reduced temperature range analyzed, the discontinuity detected at the phase transition and the presence of a plateau at low temperatures, probably associated with the relaxation of Li atoms by paramagnetic impurities.

In Fig. 6, T_1^{-1} values remain constant below 250 K, indicating that time spent by Li at Li(1) sites is important. Above this temperature, the residence time at these sites becomes shortened and the mobility of the lithium increases. From the linear part of the T_1^{-1} curve, detected below the phase transition temperature, a microscopic activation energy $E_m = 0.43$ eV, was deduced for the Li motion in the triclinic phase. This value is lower than that obtained with impedance spectroscopy[5] ($E_M = 0.65$ eV), suggesting the existence of correlation effects on the lithium motion. According to Ngai's work,[21] the long-range activation energy E_M is given by the expression: $\beta E_M = E_m$, where E_m is the microscopic energy deduced from NMR results and β is the correlation parameter associated with the Li motion. From E_m and E_M values, a value of $\beta \approx 0.6$ was deduced. Above the phase transition, T_1^{-1} values attain a broad maximum indicating that correlation times are near $\tau_c \approx 10^{-8}$ s. In a previous work, two different relaxation mechanisms were resolved in the T_1^{-1} curve of this compound; however, long-range activation energies could not be measured precisely. From electric impedance measurements, a macroscopic activation energy of 0.43 eV could be finally measured for the high-temperature phase[5,16] of $LiZr_2(PO_4)_3$.

Along the transition, the quadrupole constant of the rhombohedral phase, $C_Q = 110$ kHz, decreases considerably with respect to that measured in the triclinic phase ($C_Q = 186$ kHz). However, C_Q values measured in the rhombohedral $LiZr_2(PO_4)_3$ phase are considerably higher than those measured[22,23] in $LiTi_2(PO_4)_3$ ($C_Q \approx 45$ kHz), where Li ions occupy M_1 sites. This difference supports the hypothesis that lithium ions occupy, besides M_1 sites, other structural sites with high C_Q values in the rhombohedral form. If it is assumed that lithium ions spend similar times at M_1 and intermediate Li(1) sites, the

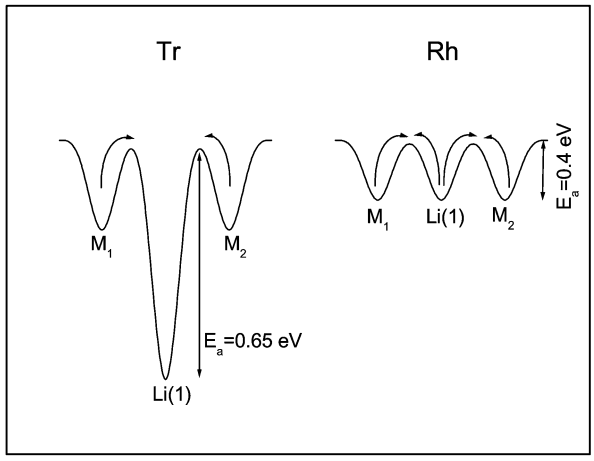

Fig. 7 Schematic diagram of potential wells along conduction paths, deduced from NMR results of the triclinic (left) and the rhombohedral (right) phases.

measured quadrupole constant will be given in the fast exchange approximation, by the expression[4]

$$C_Q = \frac{C_Q^A P_A + C_Q^B 3P_B}{P_A + 3P_B}$$

where C_Q^A and C_Q^B are the quadrupole constants of M_1 and Li(1) sites, P_A and P_B are the occupation probabilities of M_1 and Li(1) sites, and the factor 3 takes into account the multiplicity of Li(1) sites. However, the calculated value ($C_Q \approx 145$ kHz) is higher than that deduced from the NMR spectrum (110 kHz), suggesting that Li occupies sites with lower C_Q constants [M_2 or Li(2)] or that C_Q values of the Li(1) sites decreased above the phase transition. The structural analysis of two phases of $LiZr_2(PO_4)_3$ showed that Li(1)–O distances increase when going from the triclinic to the rhombohedral form, supporting the assumed decrease of C_Q in Li(1) sites. Above the phase transition, C_Q values do not change, indicating that P_A and P_B must be near 0.25 (the maximum delocalisation of lithium).

Taking into account the results obtained in this work, the schematic diagram of potential wells given in Fig. 7 can be tentatively proposed. In the triclinic phase, Li^+ ions occupy the potential wells associated with Li(1) sites and the resulting mobility is very low. According to this fact, the four-fold coordination of Li at Li(1) sites, deduced from ND data, could be responsible for the triclinic distortion detected in $LiZr_2(PO_4)_3$. Above 310 K, coordination of Li becomes uncomfortable at the Li(1) sites and potential wells at Li(1) sites decrease producing the triclinic–rhombohedral transformation. In the rhombohedral form, potential wells of Li(1) decrease and become similar to that of the M_1 sites; from this fact, residence times at M_1 and Li(1) sites become similar, favoring exchange processes between these sites and the delocalisation of lithium in conduction paths. Taking into account the important amount of vacant sites in conduction channels and that structural bottlenecks along conduction paths do not limit Li diffusion, the resulting mobility of Li is important in the rhombohedral phase. The existence of frequent hops between Li(1) and M_1 sites explains the averaged rhombohedral symmetry detected by NMR and the difficult localization of Li by ND technique.

Conclusions

The triclinic–rhombohedral transformation of $LiZr_2(PO_4)_3$ produced at 310 K has been studied by DSC, XRD and ^{31}P MAS-NMR techniques. Along the transition, a hysteresis loop was detected in which both crystallographic phases coexist.

This last point supports the martensitic character of the first-order analyzed transition.

The use of ^{7}Li NMR spectroscopy has permitted the analysis of structural sites occupied by Li^+ ions in the two structural forms of $LiZr_2(PO_4)_3$. From the analysis of quadrupole parameters ($C_Q = 186$ kHz, $\eta = 0$), the four-fold coordination of Li at Li(1) sites, deduced from the ND study of the triclinic phase, has been confirmed. In this phase the activation energy deduced from Li NMR data is $E_a = 0.43$ eV; however, correlation effects on Li motion increased to $E_M = 0.65$ eV, the macroscopic activation energy deduced from conductivity measurements. Above the phase transition, residence times at structural sites decreased, favoring delocalization of Li ions in conduction paths. As a consequence of the averaging motions, an axial symmetry was deduced from the ^{7}Li NMR spectrum of the rhombohedral phase ($C_Q = 110$ kHz, $\eta = 0$). The important mobility of lithium, explains the difficulties found studying the localization of lithium in the rhombohedral phase by diffraction techniques.

Acknowledgements

Financial support provided by CICYT, projects MAT98-1053-C04-03 and MAT2001-3713-C04-03 is gratefully acknowledged. K. A. thanks AECI for the fellowship received.

References

1 J. B. Goudenough, H. Y.-P. Hong and J. A. Kafalas, *Mater. Res. Bull.*, 1976, **11**, 203.
2 J. M. Winand, A. Rulmont and P. Tarte, *J. Solid State Chem.*, 1991, **93**, 341.
3 A. Martinez-Juárez, J. M. Rojo, J. E. Iglesias and J. Sanz, *Chem. Mater.*, 1995, **7**(10), 1857.
4 M. A. París, A. Martínez-Juárez, J. E. Iglesias, J. M. Rojo and J. Sanz, *Chem. Mater.*, 1997, **9**, 1430.
5 F. Sudreau, D. Petit and J. P. Boilot, *J. Solid State Chem.*, 1989, **83**, 78.
6 A. Martinez-Juárez, C. Pecharromán, J. E. Iglesias and J. M. Rojo, *J. Phys. Chem. B*, 1998, **102**, 372.
7 M. Alami, R. Brochu, J. L. Soubeyroux, P. Graverau, G. le Flem and P. Hagenmuller, *J. Solid State Chem.*, 1991, **90**, 185.
8 D. Tran Qui, S. Hamdoune, J. L. Soubeyroux and E. Prince, *J. Solid State Chem.*, 1988, **72**, 309.
9 E. Morin, J. Angenault, J. C. Couturier, M. Quarton, H. He and J. Klinowski, *Eur. J. Solid State Inorg. Chem.*, 1997, **34**, 947.
10 E. R. Losilla, M. A. G. Aranda, M. Martinez-Lara and S. Bruque, *Chem. Mater.*, 1997, **9**, 1678.
11 M. Catti, S. Stramare and R. Ibberson, *Solid State Ionics*, 1999, **123**, 173.
12 J. E. Iglesias and C. Pecharromán, *Solid State Ionics*, 1998, **112**, 309.
13 M. Catti and S. Stramare, *Solid State Ionics*, 2000, **136–137**, 489.
14 D. Massiot, WINFIT, Bruker-Franzen Analytik GmbH, Bremen, Germany, 1993.
15 J. Alamo and J. L. Rodrigo, *Solid State Ionics*, 1989, **32/33**, 70.
16 C. P. Slichter, *Principles of Magnetic Resonance*, 3rd edn., Springer, Berlin, 1990.
17 J. H. Van Vleck, *Phys. Rev.*, 1978, **74**, 1168.
18 D. Petit and B. Sapoval, *Solid State Ionics*, 1986, **21**, 293.
19 M. Grüne and W. Müller-Warmuth, *Phys. Chem.*, 1991, **95**, 1068.
20 O. Kanert, R. Küchler, K. L. Ngai and H. Jain, *Phys. Rev. B*, 1994, **49**, 76.
21 K. L. Ngai, *Phys. Rev. B.*, 1993, **48**, 13 481.
22 M. A. París, A. Martinez-Juárez, J. M. Rojo and J. Sanz, *J. Phys.: Condens. Matter*, 1996, **8**, 5355.
23 K. Arbi, S. Mandal, J. M. Rojo and J. Sanz, *Chem. Mater.*, 2002, **14**, 1091.